Materials Physics and Mechanics 47 (2021) 65-73 Received: December 21, 2020

EFFECT OF PROCESS PARAMETERS ON THE CRYSTAL-PARAMETERS OF Cu-Zn SPINEL-FERRITES

Naveen Kumar*, Ajaya Bharti, Abhishek Kumar, Abhishek Nigam

Applied Mechanics Department, Motilal Nehru National Institute of Technology Allahabad, Prayagraj-211004, India

*e-mail: chaudhary56naveen@gmail.com

Abstract. Spinel ferrite nano-powders are highly useful in applications such as drug-delivery, ferrofluids, gas sensors, etc. because of their semiconductor and ferromagnetic properties. There are various methods by which the spinel ferrites can be synthesized, i.e., hydro-thermal route, solid-state route, sol-gel route, thermal deposition route, mechanical milling, etc. In this work, nano-crystalline Cu-Zn ferrites with the composition of ($Cu_{0.4}Zn_{0.6}Fe_2O_4$) were synthesized from metal nitrate and acetate precursors by the hydro-thermal route and sol-gel auto-combustion route. Citric acid was used as a fuel to increase the rate of reaction. Synthesized powders were heat-treated for different holding time. The crystal structures of these compounds were characterized by X-ray diffraction (XRD). The crystal size and lattice parameter were determined by using Maud analysis and Williamson-hall plots. The Rietveld analysis and X'Pert Highscore peak match analysis confirmed the formation of single-phase $Cu_{0.4}Zn_{0.6}Fe_2O_4$. It was observed that crystallite size and peak intensity increased after heat treatment. Also, on increasing the holding time of heat treatment, an increase in the peak intensity and crystallite size was observed.

Keywords: copper, zinc, spinel ferrite, hydro-thermal, sol-gel, heat-treatment

1. Introduction

The high surface to volume ratio of nano-ferrites powders has attracted the attention of researchers and industries throughout the world [1]. The formula of cubic spinel ferrite is $XYFe_2O_4$, where X and Y are substituted metals such as Cu, Zn, Ni, Co, etc. [2,3]. Spinel ferrite exhibits semiconductor and ferromagnetic properties [4]. Spinel ferrite nano-powders are highly useful in applications, i.e., drug-delivery, ferrofluids, gas sensors, etc. because of their magnetic nature [5,6]. Spinel-ferrites can also be used to fabricate polymer matrix composites or metal matrix composites [7-11]. There are various methods by which the spinel ferrites can be synthesized, i.e., hydro-thermal route, solid-state route, sol-gel route, thermal deposition route, mechanical milling, etc. [12,13]. Hydro-thermal route and sol-gel are the most commonly used methods for the fabrication of spinel ferrite due to the ease of fabrication of single-phase material [14,15]. Properties of fabricated spinel ferrite powders are highly dependent on the heat treatment process. Different types of heat treatments (i.e., annealing, normalizing, etc.) of nano-ferrites powder are done to achieve the required properties. Annealing is the most commonly used heat treatment process for nano-ferrites.

Kavas et al. synthesized the Zn substituted Cu-ferrite by sol-gel auto-combustion route [16]. It was observed that the lattice parameter increased continuously with an increase in Zn content. Wu et al. fabricated the Cu-Zn spinel ferrite by thermal deposition method [17]. Highly crystalline spherical $Cu_{0.5}Zn_{0.5}Fe_2O_4$ was obtained after calcination at 600°C for 2 hrs.

http://dx.doi.org/10.18149/MPM.4712021_7

Baykal et al. investigated the optical and magnetic properties of Cu-Zn spinel ferrite dispersed in silica fabricated by the sol-gel route [18]. XRD analysis approved the phase purity of fabricated powder. Lattice parameters were found to be lying in between the lattice parameters of Cu-ferrite and Zn-ferrite. Rana et al. investigated the effect of Zn substitution on the magnetic and microstructural properties of Cu-Zn ferrite fabricated by a solid-state route [19]. Single-phase particles were formed, and grain size reduced with an increase in the zinc content. Tangcharoen et al. investigated the effect of Zn doping on the magnetic properties of metal ferrites fabricated by the sol-gel route [20]. Slight peak shifting was observed on the addition of Zn.

The general formula of Cu-Zn spinel ferrites is $Cu_{(1-x)}Zn_xFe_2O_4$. The infinite number of Cu-Zn spinel ferrite can be obtained by varying the X value [21]. In this work, nano-crystalline Cu-Zn ferrites with the composition of ($Cu_{0.4}Zn_{0.6}Fe_2O_4$) were synthesized from metal nitrate and acetate precursors by the hydro-thermal route and sol-gel auto-combustion routes. The fabricated powder was heat-treated to different holding times. The effect of heat-treatment time was studied on the properties of $Cu_{0.4}Zn_{0.6}Fe_2O_4$.

2. Experimentation

Materials Used. Materials used in the present work are copper nitrate ($Cu(NO_3)_2.3H_2O$), iron nitrate ($Fe(NO_3)_2.9H_2O$), zinc acetate ($(CH_3COO)_2Zn.2H_2O$), citric acid, and sodium hydro-oxide (NaOH). Data of precursors used during the synthesis of Cu-Zn nano-ferrite powders is given in Table 1.

Table 1. Properties of precursors

Salts	M_w	Purity
$Cu(NO_3)_2.3H_2O$	241.60	99.5-102 %
$Fe(NO_3)_2.9H_2O$	404.00	98 %
$(CH_3COO)_2Zn.2H_2O$	219.49	98 %
$C_6H_8O_7.H_2O$	211.14	99 %

Calculations for the Weight of Precursors. The weight of precursors used during the synthesis of powders was calculated based on the balanced chemical reaction given in Equation 1. It can be seen from the equation that the one mole of $Cu_{0.4}Zn_{0.6}Fe_2O_4$ requires 0.4 moles of copper nitrate, 0.6 moles of zinc acetate, 2 moles of iron nitrate, and 4.5 moles of citric acid.

$$0.4Cu(NO_3)_2.3H_2O + 0.6(CH_3COO)_2Zn.2H_2O + 2Fe(NO_3)_2.9H_2O + 4.5C_6H_8O_7.H_2O = Cu_{0.4}Zn_{0.6}Fe_2O_4 + Gases\ (as\ by-products). \quad (1)$$

The weight of precursors required was calculated based on molecular weight (Mw), purity, and the number of moles (required for one mole of $Cu_{0.4}Zn_{0.6}Fe_2O_4$). Formula to calculate the weight of precursors required for Wp gram of $Cu_{0.4}Zn_{0.6}Fe_2O_4$ is given below in Equation 2.

$$Weight\ of\ Precursor\ Required = \frac{Mw\ of\ Precursor \times Wp \times Coefficent \times 100}{Mw\ of\ powder\ to\ be\ synthesized \times Purity}. \quad (2)$$

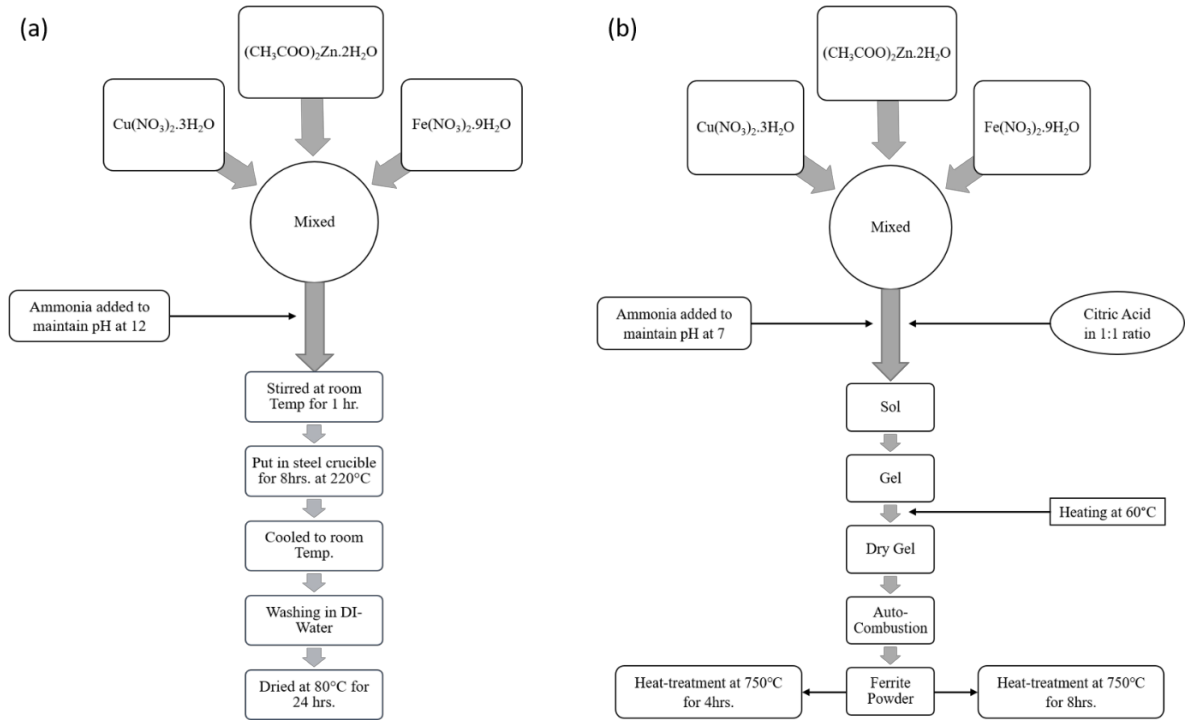

Fig. 1. Flowchart for (a) hydro-thermal route and (b) sol-gel route

Methodology. Nano-powders were fabricated by two different routes, i.e., hydro-thermal route and sol-gel route. Flowchart for the fabrication of Cu-Zn nano-ferrite by the hydro-thermal route and sol-gel route is given in Fig. 1 [22]. The powder fabricated by the sol-gel route was annealed at 750°C for two different holding times (4hrs. and 8hrs.). Details of prepared samples are given in Table 2.

Table 2. Sample Preparation

Processing Route	Sample Code
Hydro-thermal route	A
Sol-gel route followed by heat-treatment at 750°C for 4hrs	B1
Sol-gel route followed by heat-treatment at 750°C for 8hrs	B2

Characterization. Prepared powders, i.e., A, B1, and B2 were characterized using X-ray Diffraction (XRD) and Scanning Electron Microscopy (SEM). XRD patterns were analyzed using peak match analysis (X'Pert Highscore), Williamson-Hall plot analysis, and Rietveld analysis (Maud). Peak matching analysis of the XRD pattern of prepared powders was done to know the presence of various phases. Rietveld analysis and Williamson-hall plot analysis were done to know the crystallite size and lattice parameters of prepared samples.

3. Results and Discussion

X-ray Diffraction (X'Pert Highscore). Figure 2 shows the indexed XRD patterns of fabricated powders.

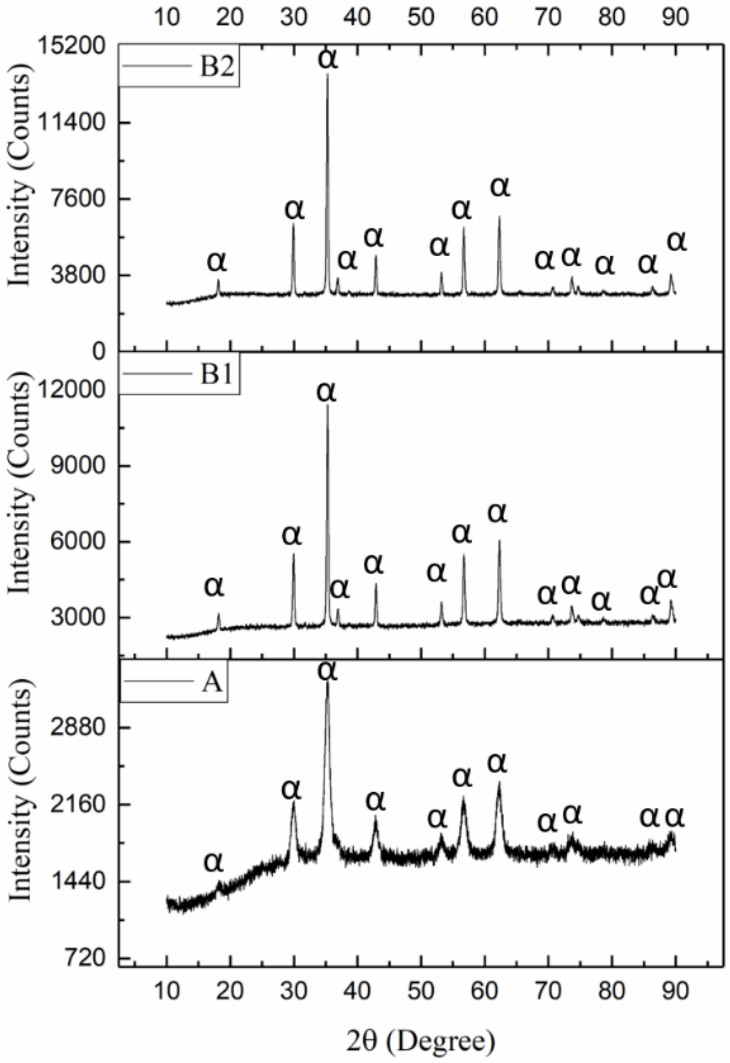

Fig. 2. Indexed XRD patterns of fabricated powders

Peak match analysis confirmed the formation of single-phase Cu-Zn nano-ferrite in all three samples, i.e., A, B1, and B2. It can be observed from Fig. 2 that the baseline of sample A is thick; this shows that the material is amorphous. The baseline of samples B1 and B2 was thin; this shows the high crystallinity in the material. The peak intensity of the XRD pattern also increased after the heat treatment of powders. An increase in peak intensity is due to the alignment of grains in one direction, and an increase in crystallite size. Peak broadening can also be observed in the untreated powder (sample A); this can also be due to the small crystallite sizes. So, the heat treatment of powders increased the crystallinity in the material.

Scanning Electron Microscopy. SEM images of samples A, B1, and B2 at different scales and magnification are shown in Fig. 3. It can be seen from Fig. 3 that the sub-micron particles were agglomerated to form the big particles in the case of all the samples A, B1, and B2. But, the agglomeration in the case of sample A (hydrothermal route) was high in comparison to sample B1 and B2 because no heat treatment was done for this sample. Sample B1 and B2 were heat-treated, because that particles did not stick to each other and that resulted in less agglomeration of particles.

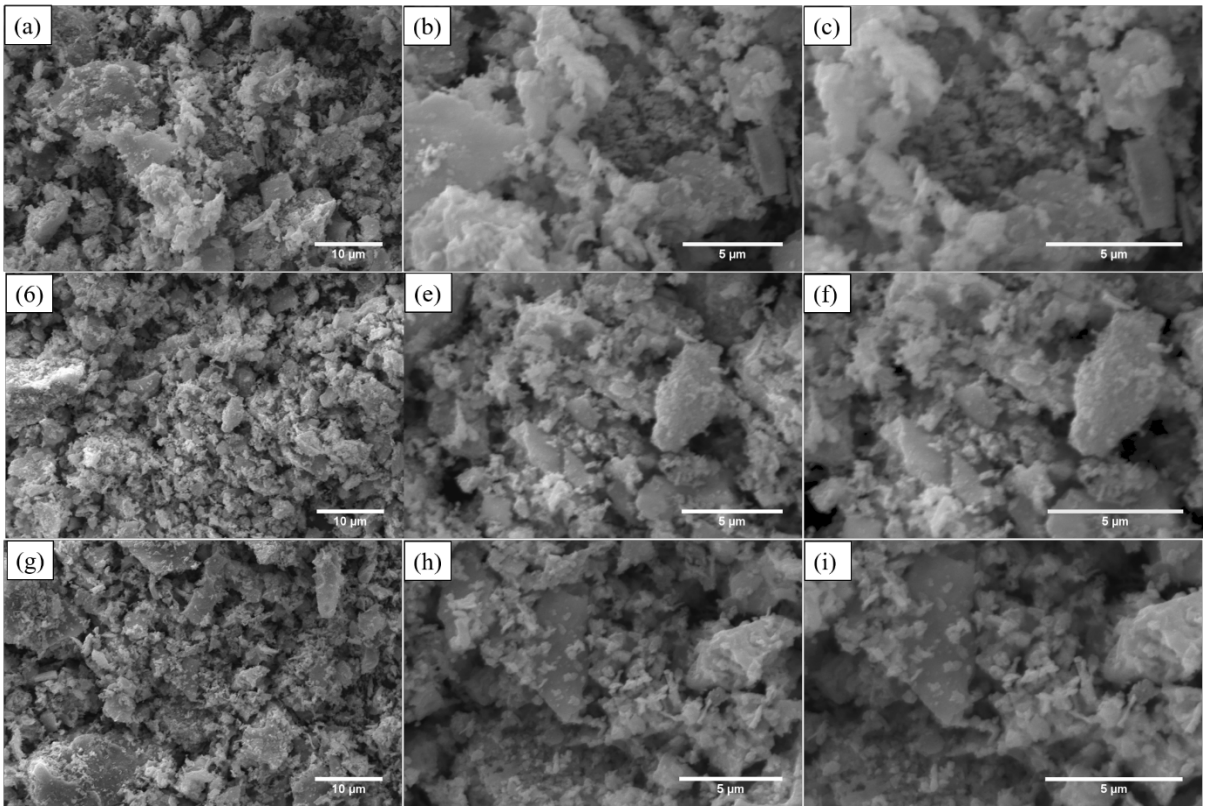

Fig. 3. SEM images of (a-c) sample A, (d-f) sample B1, and (g-h) sample B2

Williamson-Hall Plot Analysis. Williamson-Hall plots of all three samples are given in Fig. 4. Williamson-Hall plot is used to find out the crystallite size and lattice strain in the samples. The slope of BCosθ vs. Sinθ gives the value of the lattice strain, while the intercept gives the value of crystallite size.

$$BCos\theta = \varepsilon Sin\theta + k\lambda/L, \quad (3)$$

$$y = mx + c. \quad (4)$$

Equation 3 is the showing the relationship between the crystallite size (L) and Bragg's angle θ. While Equation 4 is the general equation of the line. On comparing Equation 3 with Equation 4, slope (m) is equal to lattice strain (ε), and intercept (c) is equal to kλ/L. Where, k is a constant and equals 0.9 or 1 and λ is the wavelength. The value of crystallite size and lattice strain for all the samples is shown in Table 3. It can be observed that the crystallite size increased after the annealing. Also, lattice strain reduced after the annealing. The reason for the increased crystallite size and reduced lattice strain is the recrystallization and grain growth in the material.

Table 3. Crystallite size and lattice strain of samples calculated using Williamson-Hall plot

Sample	Crystallite Size (Å)	Lattice Strain
A	129.89	0.0064
B1	329.21	0.0016
B2	352.67	0.0019

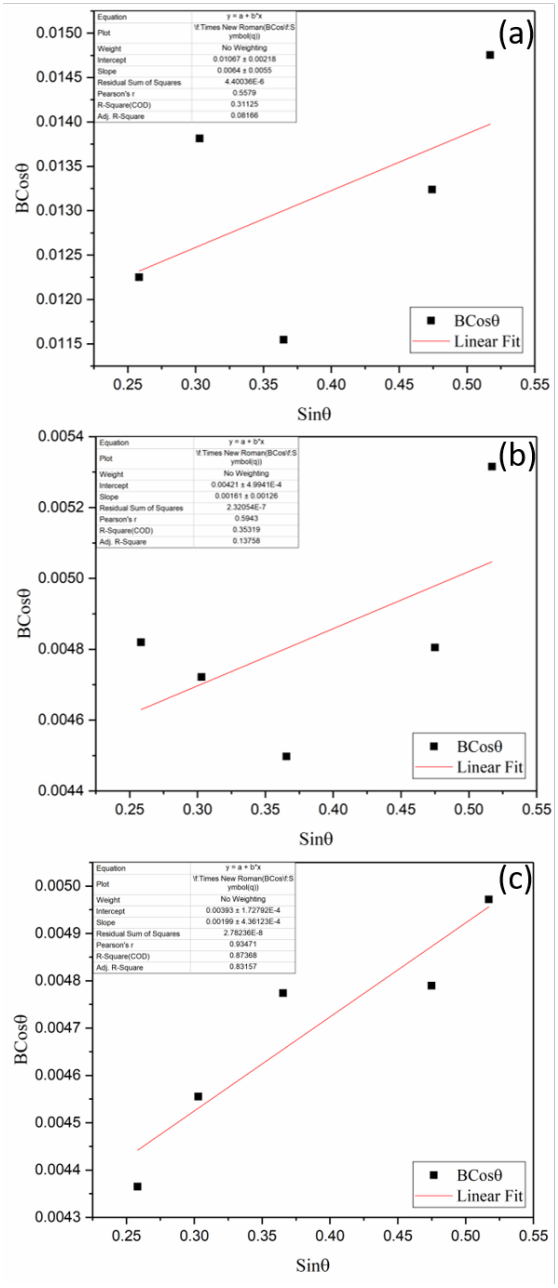

Fig. 4. Williamson-Hall plots of (a) A (b) B1, and (c) B2

Rietveld Analysis. Rietveld analysis of the fabricated powders was done by matching the XRD peaks with the standard peak (CIF File: 9012442). Figure 5 shows the Maud analyzed XRD patterns of the fabricated powders. It can be observed from Fig. 5 that all the peaks matched perfectly with the standard XRD pattern (CIF File: 9012442); this confirms the formation of single-phase Cu-Zn nano-ferrite. The crystallite size and lattice parameter of all the three powders obtained after the Maud analysis are given in Table 4. It can be observed from Table 4 that the lattice parameter remained constant with an increase in the heat-treatment time; this shows that the heat-treatment of powder does not affect the crystal structure of the material. The lattice parameter of sample A was found to be 8.436Å. While the lattice parameter of samples B1 and B2 was 8.43Å. It can also be observed from Table 4 that the crystallite size increased sharply after the heat treatment of powders. Also, on increasing the holding time of the heat-treatment, an increase in the crystallite size was observed. An increase in the crystallite was due to the grain growth and increased crystallinity

in the material. The largest crystallite size of 1090.84Å was obtained for sample B2. The Crystallite size of sample A was found to be very low (126.66Å). So, there is a difference in the value of crystallite size obtained from Rietveld's analysis and Williamson-Hall plot. But, the trend shown by both is similar. The reason for the difference in the crystallite size value can be the error present in Williamson-hall plot calculations due to linear curve-fitting.

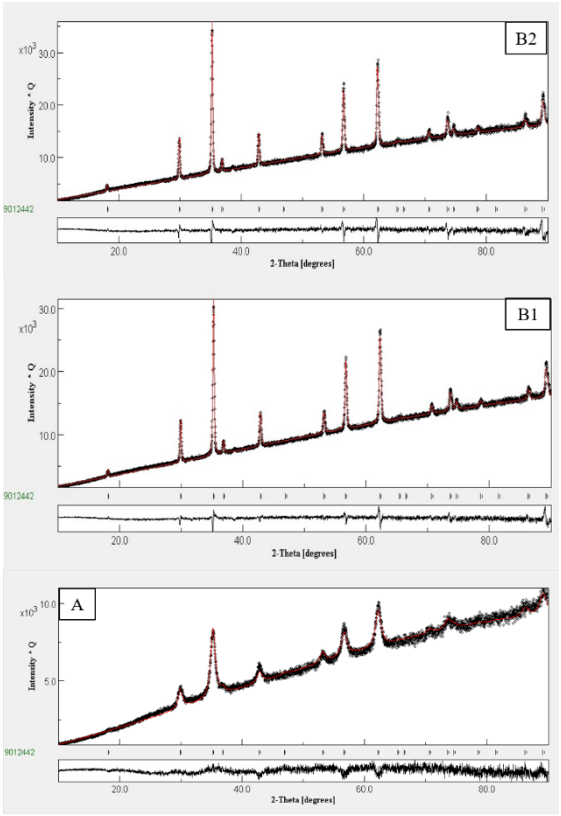

Fig. 5. Maud analysis of fabricated powders

Table 4. Crystallite size and lattice parameter of samples obtained from Maud analysis

Sample	Crystallite Size (Å)	Lattice Parameter
A	126.66	8.436
B1	1080.84	8.43
B2	1090.84	8.43

4. Conclusions

Following conclusions are drawn after the fabrication and characterization of Cu-Zn nano-ferrites fabricated by the hydrothermal route and sol-gel route followed by heat treatment:

- Both the Rietveld analysis and X'Pert Highscore peak match analysis confirmed the formation of single-phase $Cu_{0.4}Zn_{0.6}Fe_2O_4$.
- Crystallite size and peak intensity of fabricated Cu-Zn nano-ferrite powders increased after the heat treatment.
- Peak intensity and crystallite size also increased with an increase in the holding time of heat treatment.

- The lattice parameter of un-treated powder fabricated by the hydrothermal route was found to be 8.436Å. While, the lattice parameter of powder, fabricated by sol-gel route followed by heat treatment (at 750°C or 4hrs and 8hrs.) was 8.43Å.
- The largest crystallite size was obtained for the sol-gel route fabricated Cu-Zn nano-ferrite powder heat-treated at 750°C for 8hrs. The Crystallite size of un-treated powder fabricated by the hydrothermal route was the lowest.
- Lattice strain reduced after the heat-treatment of powder. Minimum lattice strain was observed for sample heat-treated at 750°C for 4hrs.

Acknowledgements. *No external funding was received for this study.*

References

[1] Maria KH, Choudhury S, Hakim MA. Structural phase transformation and hysteresis behavior of Cu-Zn ferrites. *International Nano Letters*. 2013;3: 42.
[2] Tatarchuk T, Bououdina M, Macyk W, Shyichuk O, Paliychuk N, Yaremiy I, Al-Najar B, Pacia M. Structural, Optical, and Magnetic Properties of Zn-Doped $CoFe_2O_4$ Nanoparticles. *Nanoscale Research Letters*. 2017;12: 141.
[3] Hu J, Ma Y, Kan X, Liu C, Zhang X, Rao R, et al. Investigations of Co substitution on the structural and magnetic properties of Ni-Zn spinel ferrite. *Journal of Magnetism and Magnetic Materials*. 2020;513: 167200.
[4] Aggarwal N, Narang SB. Magnetic characterization of Nickel-Zinc spinel ferrites along with their microwave characterization in Ku band. *Journal of Magnetism and Magnetic Materials*. 2020;513: 167052.
[5] Li LZ, Peng L, Zhong XX, Wang R, Tu XQ. Structural, magnetic and electrical properties of Cu-Zn ferrite nanopowders. *Journal of Magnetism and Magnetic Materials*. 2016;419: 407-411.
[6] Gao JM, Cheng F. Study on the preparation of spinel ferrites with enhanced magnetic properties using limonite laterite ore as raw materials. *Journal of Magnetism and Magnetic Materials*. 2018;460: 213-222.
[7] Kumar D, Bharti A, Azam SM, Kumar N, Tripathi H. Investigations of Mechanical Properties of Copper Matrix Hybrid Composite. In: *Advances in Mechanical Engineering*. Singapore: Springer; 2020. p.671-676.
[8] Kumar N, Bharti A, Dixit M, Nigam A. Effect of Powder Metallurgy Process and its Parameters on the Mechanical and Electrical Properties of Copper-Based Materials: Literature Review. *Powder Metallurgy and Metal Ceramics*. 2020;59: 401-410.
[9] Kumar N, Bharti A, Gupta MK. Effect of Treatments on Thermo-mechanical Properties of Epoxy based Sisal Biocomposites. *International Journal on Emerging Technologies*. 2020;11(3): 491-495.
[10] Kumar N, Bharti A, Saxena KK. A re-analysis of effect of various process parameters on the mechanical properties of Mg based MMCs fabricated by powder metallurgy technique. *Materials Today: Proceedings*. 2020;26: 1953-1959.
[11] Kumar N, Bharti A, Tripathi H. Investigation of Microstructural and Mechanical Properties of Magnesium Matrix Hybrid Composite. In: *Advances in Mechanical Engineering*. Singapore: Springer; 2020. p.661-669.
[12] Mahmoud MH, Hassan AM, Said AE-AA, Hamdeh HH. Structural; magnetic and Catalytic properties of nanocrystalline $Cu_{0.5}Zn_{0.5}Fe_2O_4$ synthesized by microwave combustion and ball milling methods. *Journal of Molecular Structure*. 2016;1114: 1-6.
[13] Yadav RS, Kuřitka I, Havlica J, Hnatko M, Alexander Cň, Masilko J, et al. Structural, Magnetic, Elastic, Dielectric and Electrical Properties of Hot-Press Sintered $Co_{1-x}Zn_xFe_2O_4$

(x=0.0, 0.5) Spinel Ferrite Nanoparticles. *Journal of Magnetism and Magnetic Materials*. 2017;447: 48-57.
[14] Parashar J, Saxena VK, Jyoti, Bhatnagar D, B.Sharma K. Dielectric behaviour of Zn substituted Cu nano-ferrites. *Journal of Magnetismand Magnetic Materials*. 2015;394: 105-110.
[15] Yadav RS, Havlica J, Hnatko M, Šajgalík P, Alexander C, Palou M, Bartoníčková E, Boháč M, Frajkorová F, Masilko J, Zmrzlý M, Kalina L, Hajdúchová M, Enev V. Magnetic properties of $Co_{1-x}Zn_xFe_2O_4$ spinel ferrite nanoparticles synthesized by starch-assisted sol–gel autocombustion method and its ball milling. *Journal of Magnetism and Magnetic Materials*. 2015;378: 190-199.
[16] Kavas H, Baykal A, Demir A, Toprak MS, Aktas B. $Zn_xCu(_{12x})Fe_2O_4$ Nanoferrites by Sol–Gel Auto Combustion Route: Cation Distribution and Microwave Absorption Properties. *J Inorg Organomet Polym*. 2014;24: 963-970.
[17] Wu W, Cai J, Wu X, Wang K, Hu Y, Wang Q. Nanocrystalline $Cu_{0.5}Zn_{0.5}Fe_2O_4$: Preparation and Kinetics of Thermal Decomposition of Precursor. *J. Supercond. Nov. Magn*. 2013;26: 3523-3528.
[18] Baykal A, Esir S, Demir A, Güner S. Magnetic and optical Properties of $Cu_{1-x}Zn_xFe_2O_4$ Nanoparticles Dispersed in a silica matrix by a solgel auto-combustion method. *Ceramics International*. 2014;41(1): 231-239.
[19] Rana MU, Abbas T. The effect of Zn substitution on microstructure and magnetic properties of $Cu_{1-x}Zn_xFe_2O_4$ ferrite. *Journal of Magnetism and Magnetic Materials*. 2002;246(1-2): 110-114.
[20] Tangcharoen T, Ruangphanit A, Pecharapa W. Structural and magnetic properties of nanocrystalline zinc-doped metal ferrites (metal¼Ni; Mn;Cu) prepared by sol–gel combustion method. *Ceramics International*. 2013;39(S1): S239-S243.
[21] Ajmal M, Maqsood A. Structural, electrical and magnetic properties of $Cu_{1-x}Zn_xFe_2O_4$ ferrites ($0 \leq x \leq 1$). *Journal of Alloys and Compounds*. 2008;460(1-2): 54-59.
[22] Abhishek N, Pawar SJ. Structural, magnetic, and antimicrobial properties of zinc doped magnesium ferrite for drug delivery applications. *Ceramics International*. 2019;46(4): 4058-4064.